Uncertainty in pore size distribution derived from adsorption isotherms: II. Adsorption integral approach

S. Hadi Madani [a], *Luis H. Diaz* [b,*], *Mark J. Biggs* [b,†], *Phillip Pendleton* [a,c,‡]

[a] Ian Wark Research Institute, University of South Australia, Mawson Lakes, SA 5095, Australia

[b] School of Chemical Engineering, University of Adelaide, Adelaide, SA 5005, Australia

[c] Sansom Institute, University of South Australia, Adelaide, SA 5001, Australia

[*] Current address: School of Engineering and Information Technology, Charles Darwin University, Darwin, NT 0909, Australia.

[†] Current address: School of Science, Loughborough University, Leicestershire, UK LE11 3TU, UK.

[‡] Corresponding Author: E-mail: Phillip.Pendleton@unisa.edu.au; Tel: +61 (0)8 8302 2188

ABSTRACT

Uncertainty in the amount adsorbed in manometric adsorption isotherm measurements is well established. Here, we extend uncertainty methodologies from adsorption isotherm data uncertainty and apply them to calculate pore size distributions based on adsorption integral methods. The analyses consider as variables: uncertainty in adsorption isotherm data, regularization parameter, molecular potential model, and the number of single pore isotherms calculated with an associated quadrature interval. We demonstrate how the calculated pore size distribution is quite insensitive to the uncertainty in experimental data, but in contrast, the uncertainty in the experimental data affects the calculated value of the optimized regularization parameter which, in turn, leads to considerable variation in the calculated pore size distribution. The calculated pore size distribution is also shown to be highly dependent on the potential model selected and on the number of single pore isotherms applied to the inversion process. We conclude and suggest a quantitative comparison between calculated pore size distributions should be discouraged unless the uncertainty in the experimental data is relatively small and, default values for regularization parameters, potential models, the number of single pore isotherms and their distribution are exactly the same for each pore size distribution evaluation.

Keywords: Adsorption; Pore size distribution; Uncertainty; Porous solids

1. INTRODUCTION

Gas adsorption measurement has been applied to a diverse range of powders and porous materials for surface characterization in terms of surface chemistry and surface density of bound functional groups, and for the determination of physical properties including: specific surface area; pore connectivity, and pore size distribution (PSD) [1]. Over the past 2-3

decades, elaborate computer programs for molecular modelling have resulted in significant advances in porous materials characterization, particularly for PSD determination.

Porous materials offer challenging experimental and theoretical demands for an unequivocal interpretation of the PSD. In most cases, the anticipated complex internal structure, due to interconnected, irregularly-shaped pores of different sizes are simplified by assuming a distribution of equivalent, regularly-shaped, entities such as slit or cylinder pores. Porous materials derived from naturally-sourced materials usually offer more complex internal structures than those developed synthetically via a well-established recipe. In addition to this, pore connectivity is not considered in PSD determination models, effect of functional groups and their distribution on the surface is ignored and interaction between neighbouring pores is neglected. Hence, calculated PSD must be regarded as "effective pore size distribution" [2]. Despite the above shortcomings and simplifying assumptions, adsorption based PSD determination methods are still considered powerful tools for PSD determination. These methods can be classified into two main categories: classical methods and the integral equation approach.

Due to differences in pore filling and fluid-solid interaction mechanisms, the classical thermodynamics-based methods for PSD determination developed separately for micropores and mesopores [3]. The more recent methods for PSD determination are based on an inversion of the adsorption integral equation; for a single component adsorptive it can be written as:

$$N(T,P) = \int_0^\infty \rho(w,T,P) f(w) dw \tag{1}$$

Here, $N(T,P)$ is the experimental adsorption isotherm data at a given temperature T and pressure P. The function $\rho(w,T,P)$ represents a series of simulated isotherms nominally as single pore isotherms or SPIs (kernels) for the same adsorptive within an ideal-shaped pore of

a specified dimension, *w*, and *f(w)* is a pore size distribution function. The integration limits as cited are typically adjusted to accommodate the minimum and maximum pore sizes to be defined via the simulated SPIs. A PSD derived from the adsorption integral equation method is classified via the approach taken to calculate the SPI. These isotherms can be developed via either molecular dynamics (MD) calculations, a Monte Carlo (MC) simulation, or using a Density Functional Theory approach. The inversion of the adsorption integral equation is independent of the SPI-generation method.

The MD method solves Newton's equations of motion to calculate velocities and positions of a set of particles that are adsorbed by a simulated porous solid [1]. In MC simulation, SPIs are calculated by using a Grand Canonical ensemble (GCMC) as a μVT ensemble [4]. This method usually has shorter processing times compared to the MD method. The density functional theory correlates the whole system energy (Grand Potential Energy or GPE) as a function of particle density distribution within the system. The particular density distribution of particles that minimizes the GPE is considered to be the equilibrium density distribution [2]. DFT calculations require considerably less computational time than MD or MC methods, and yields equivalent equilibrium predictions. Wu presented a review of DFT applied to various molecular simulations [5].

Evans *et al*. introduced DFT to model gas adsorption as capillary condensation in well-defined pores [6, 7], with the method subsequently extended by Seaton *et al*. using a local DFT to define the PSD in a porous activated carbon [8]. Lastoskie *et al.* [9] modified this approach using a non-local DFT (NLDFT) model proposed by Tarazona *et al.* [10] for PSD calculation. A comparison of these methods indicates the provision for short-ranged correlations in the fluid density within the NLDFT yields a superior estimation of adsorbed phase density. This method has been widely used for PSD determination in the literature and

is now adopted as a standard for PSD analysis by the International Standard Organization (ISO) [11].

The NLDFT and previous molecular modelling methods assumed homogeneous, structurally smooth pore walls at the atomic scale. As a consequence of this simplifying assumption, NLDFT-modelled SPIs exhibit steps corresponding to molecular layering effects, eventually resulting in the appearance of artificial gaps in the calculated PSD. Neimark and co-workers later proposed the Quenched Solid Density Functional Theory (QSDFT) for silica-based [12] and carbon-based [13] materials by accounting for surface heterogeneity and roughness effects as a distribution of solid atoms on the surface and via the introduction of a single roughness parameter. The resulting SPIs for nitrogen and argon resulted in “smoother” isotherms with no layering steps, and a superior fit to the experimental data [14]. Landers *et al*. provide a review of recent advances in DFT methods for porous material characterization [15].

An application advantage of the adsorption integral equation method over the classical thermodynamics-based methods for PSD analysis derives from the uninterrupted range of pore sizes, from the smallest micropore to the largest mesopore, based on a gas adsorption isotherm from the lowest measureable relative pressure up to saturation. A disadvantage is due to the limited number of SPI libraries available in the literature confined to a few adsorptives at specific temperatures. Nonetheless, since the integral methods accommodate the entire (nitrogen-based) pore size distribution(s) and pedagogically are based on fewer initial assumptions compared to classical methods, the adsorption community is accepting them as standard characterization methods.

For gas adsorption analysis of adsorbents, we suggest that at least two distinct categories of uncertainties need to be recognized. Experimental data uncertainty is the variation of the actual measured parameter leading to a combined uncertainty in the experimental result. Only

a few studies of adsorption uncertainty are available in the literature. Loebenstein and Deitz introduced large dead-spaces in sampling tubes as the main sources of uncertainty in adsorption data [16]. Ross and Olivier addressed uncertainty corresponding to apparatus calibration [17]. Robens *et al.* investigated the non-ideal behaviour contributions of helium and nitrogen [18]. The effect of liquid nitrogen level control on adsorption results was first reported by Killip *et al.* [19]. Badalyan and Pendleton built an automated manometric gas adsorption apparatus, calibrated dosing and sample volumes and propagated uncertainty for each adsorption isotherm result [20, 21]. They introduced sample mass measurement, liquid nitrogen-level control, and dead-volume determination as the main sources of uncertainty in experimental data. Secondly, further analysis derived from the isotherm data, such as BET specific surface area, α_S-analyses, and pore volume showed an increase in their respective values [22, 23]; PSD analysis would also introduce additional combined uncertainty. Recently Caguiat *et al.* suggested an interpretation of PSD in nanoporous adsorbents. They suggested that a proper interpretation of the PSD relies on the correct selection of SPIs and adsorptives [24]. Their study examined four different carbon porous materials and their PSDs were calculated by using commercial and DFT theory.

In contrast with uncertainty in PSD analyses due to the application of classical thermodynamics methods [25], the present work begins by identifying the optimum parameters for the inversion of the adsorption integral equation to define an optimized PSD. To make a parametric analysis, we consider holding all but one of the variables constant at the optimized value, then examine the effect of variation of the variable on the resulting PSD. In some cases, it was necessary to adjust two of the variables to fully appreciate the impact of change on the resulting PSD. The variables considered were the combined standard uncertainty in the amount adsorbed, the value of the regularization parameter, the molecular model employed to calculate the SPIs, and the influence of the number of SPIs on the PSD.

2. METHODS

2.1. Experimental measurements

Single sheet, plain-weaved activated carbon cloth (ACC) FM1/250 (*ex*. Calgon Carbon, Pittsburgh, PA, USA) was used as it showed a narrow PSD in the micropore range [26]. Samples were degassed prior to the experiments at 200 ºC and a background vacuum of 0.1 mPa for 8 h. Thermal transpiration effects were accounted for at pressures below 266 Pa. Throughout the adsorption–desorption process the liquid nitrogen level was controlled constant ± 0.15 mm. Ultra-high purity (99.999%) helium and nitrogen (*ex*. BOC Gases, Adelaide, Australia) were used for dead-space measurements and adsorption experiments, respectively. The adsorption isotherm data were obtained using the adsorption apparatus presented in [20], and the uncertainty in the amount adsorbed propagated from the measured volumes and pressures using these authors' methods [21].

2.2. Theoretical approach

The theoretical approach consisted of two stages: firstly, a MC simulation method to calculate the SPIs, and secondly, an integral inversion procedure to calculate the PSD.

2.3. Simulation methods

A set of local isotherms was calculated for nitrogen adsorbed by a simulated carbon pore system using a GCMC algorithm [4]. In all cases, the simulation was regarded as equilibrated after $\geq 5 \times 10^5$ moves (or iterations) with a similar number of moves required to calculate the amount adsorbed at each pre-defined pressure. The isotherms were calculated for a carbon containing slit-shaped pores. The pore model was a smooth, parallel-surfaced slit comprised of ordered carbon atoms. The interaction potential (energy), u_{sf} , for each nitrogen (particle), *f*, with the surface, *s*, was evaluated via a Steele function defined in Eq (2):

$$u_{sf} = 2\pi\rho_s\sigma_{sf}^2\varepsilon_{sf}\left[\frac{2}{5}\left(\frac{\sigma_{sf}}{z}\right)^{10} - \left(\frac{\sigma_{sf}}{z}\right)^{4} - \frac{\sigma_{sf}^4}{3\Delta\left(z+0.61\Delta\right)^3}\right] \quad (2)$$

where, ρ_s is the surface density of the carbon centre (38.2 nm^{-2}), Δ is the interlayer spacing between two adjacent graphene layers (0.3354 nm), z is the distance of the particle centre normal to the surface plane, σ_{sf} and ε_{sf} are the cross solid-fluid molecular parameters calculated using the Lorentz-Berthelot rule. The Lennard-Jones (L-J) parameters for carbon are σ_{ss} = 0.34 nm and ε_{ss} = 28 K.

Considering the shape of the nitrogen molecule, either of two distinct L-J potential models could be used for SPI simulation: a single-centre model or a two-centre model. For the former, the collision diameter (σ_{ff}) and well depth (ε_{ff}) parameters are 0.3615 nm and 101.5 K, respectively [27]. For the latter, the two centres are each nitrogen atom 0.11 nm apart, with σ_{ff} = 0.331 nm and ε_{ff} = 36 K. This model also accounts for charge distribution as + 0.963e at the centre and – 0.482e at each edge along the N≡N axis (as the L-J sites) [28].

The fluid-fluid interaction potential was calculated by Eq (3),

$$u_{ij} = \sum_{a=1}^{A}\sum_{b=1}^{B}\frac{q_i^a q_j^b}{4\pi\varepsilon_0 r_{ij}^{ab}} + \sum_{c=1}^{C}\sum_{d=1}^{D}4\varepsilon_{ij}^{cd}\left[\left(\frac{\sigma_{ij}^{cd}}{r_{ij}^{cd}}\right)^{12} - \left(\frac{\sigma_{ij}^{cd}}{r_{ij}^{cd}}\right)^{6}\right] \quad (3)$$

where u_{ij} is the interaction energy between fluid molecules i and j. A and B are the number of charges on the molecules i and j, and C and D are the number of L-J sites on the molecules i and j. Also, ε_0 is the permittivity of a vacuum, r_{ij}^{ab} is the separation between the charge a on molecule i and the charge b on molecule j having charges q_i^a and q_j^b respectively, and r_{ij}^{cd} is the separation between the L-J site c on molecule i and the L-J site d on molecule j with combined L-J well depth of ε_{ij}^{cd} and combined L-J collision diameter of σ_{ij}^{cd} for the two sites.

2.4. Integral Inversion procedure

The inversion of the integral within Eq (1) can be made as a matrix application [29]:

$$N = AWF \tag{4}$$

where N is a vector including amount adsorbed values from the measured adsorption isotherm, W is a diagonal matrix, defined by Eq (5), wherein its non-zero components are calculated from spaces between two adjacent quadrature intervals, and A is a matrix consisting of the SPIs.

$$W = diag\left(w_{j+1} - w_j\right) \tag{5}$$

Each column in A includes an isothermal amount adsorbed for a single pore with a size equal to the average corresponding quadrature interval, w_j. Each SPI would be calculated (or interpolated) for the entire pressure range of the isotherm. The term F is the PSD function vector. From Eq. (4), the solution for F would be calculated by minimizing the residuals function:

$$R = \left(N - AWF\right)^T \left(N - AWF\right) \tag{6}$$

Two mathematical dilemmas exist for the inversion of the integral in Eq. (1) via the minimization of the residuals in Eq. (6). Firstly, Eq. (1) is mathematically ill-conditioned and any subtle changes in the experimental data (N) could result in a substantially different PSD (F). Secondly, the PSD function would be expected to be a continuous function with relatively smooth peaks. A solution of this system as presented on Eq (6) would actually result in a spiky PSD, regarded as a mathematical artefact [29]. These undesirable effects can be removed by applying an appropriate regularization method, such as that due to Tikhonov [30-32]. In the current work, regularization was incorporated in the PSD calculation by adding the smoothing term (αS) to the residual in Eq. (6), where S is a discrete second

derivative of the PSD function (F) and α is an adjustable coefficient known as the "regularization parameter", associated with the degree of smoothness.

$$R = \left(N - AWF\right)^T \left(N - AWF\right) + \alpha S \tag{7}$$

3. RESULTS AND DISCUSSION

Inversion of the integral in Eq (1) is the core of the analysis towards a PSD. The discussion below presents our procedures to initially produce what we regarded was the optimum PSD for the activated carbon cloth. We discuss the methods employed to define the optimum value for the smoothing coefficient α used in the regularisation expression Eq. (7). The optimised PSD is subsequently derived then used as the basis for parametric analyses. Variables to be discussed include: adsorbed volume uncertainty, regularisation parameter, molecular (simulation) model, and the number of SPIs.

3.1. Experimental isotherm

Figure 1 shows the high-resolution nitrogen adsorption isotherm for FM1/250 activated carbon at 77K. Low pressure data is also included for clarity. The sample exhibits classical type I isotherm based on IUPAC classification [33] indicating highly microporous structure with negligible contribution of mesopores. The figure includes the uncertainty associated with the amount adsorbed at each pressure point as vertical intervals [21]. Since the data were collected progressively with increasing equilibrium pressure, the uncertainty in each adsorption point accumulates.

3.2. Integral inversion results

A total of 53 calculated SPIs for nitrogen adsorbed by carbon slit-shaped pores were considered at equilibrium after ≥ 5 x 10^5 configurational moves, with each SPI regarded as exact and accurate with no associated, discernable uncertainty. Thus, the SPIs do not

contribute to the uncertainty of a calculated PSD. The only simulation source of uncertainty would be the molecular model and the number of SPIs used in the fitting process.

The minimization of the first term in Eq (7) would improve the experimental data fitting but also produce an unstable, spiky PSD with sharp peaks. If the second term were to be minimized this would result in wider peaks and a smoother and more stable PSD but with a poorer experimental data fit. Some peaks may disappear as a result of regularization and some closely-located peaks may merge to form a single peak with a maximum at a value between the two initial peaks. Clearly, the objective is to select a regularization parameter that leads to a relatively smooth and stable PSD and with a relatively good fit of the experimental data. Davies *et al*. suggested two possible methods to obtain an optimum regularization parameter: the "fitting error" method and/or the "Generalized Cross Validation" (GCV) method [29].

The fitting error method uses a plot of the error as a function of regularisation parameter α (Figure 2). The plot shows an almost constant error value from low α values up to a threshold value above which the error increases substantially with α. The optimum α value would be identified as the threshold value. The shape of the curve is very similar to surface tension-(log) concentration plots to identify the critical micelle concentration; intersection of two linear imprints on the curve yields a value for $\alpha = 4.64 \times 10^{-7}$.

The GCV method is based on the premise that the optimum-valued regularisation parameter can be defined via a balance between closeness of (data) fit and complexity. The former is simply the residual sum of squares; a decrease in the number of variables applied to the selected model would reduce complexity [32]. Such analysis yields a minimum in the GCV source function located at the optimum α value = 4.64×10^{-7}.

The PSD was calculated using the optimum regularisation parameter in conjunction with the fitting error plot and the GCV score function plot [29, 34].

Inversion of Eq (1) via Eq (2), with an application of the optimum-valued regularization parameter α (=4.64 x 10^{-7}) and SPI models based on the double site and charges model, gave the PSD shown in Figure 3. The resulting distribution indicates the principal volume of pores were contained in the range 1.2 ± 0.15 nm with secondary volumes contained in pores ranging from 1.7 ± 0.1 nm to 2.3 ± 0.1 nm. A parametric analysis of the PSD is focused on the principal volume of pore's peak. The presence of the secondary volume of pores' peaks could be a result of contributions from one or more of at least three sources: the porous nature of the adsorbent; the regularisation parameter value selected; or, the optimisation procedure used to solve the AIE. Deconvolution of this trio of contributions will be the subject of a future publication.

3.3. Parametric analysis

We have calculated the PSD based on the experimental data and a set of SPIs obtained from simulation. This method is similar to those used as an analytical function in commercial adsorption characterization equipment. The following represents a parametric analysis of our (*ergo* the commercial) routines for calculating a PSD, where PSD = $f(u_C(V_i)$, α, molecular potential model, number SPIs). Within each analysis, only one of the variables is considered with the remainder held either constant or at the optimised values.

3.3.1. Effect of the uncertainty in amount adsorbed on the PSD

For this analysis, α, molecular model, and the number of SPIs were the optimised values (for isotherm data set p_i, V_i) and maintained constant. Figure 1 shows that for each pressure point, p_i, there is an uncertainty in the amount adsorbed ΔV_i. Each amount adsorbed, V_i, is located between the minimum amount adsorbed $V_i - \Delta V_i$ and the maximum $V_i + \Delta V_i$, whence V_i is the usual amount adsorbed reported in the literature. The PSDs calculated for isotherms

represented by (p_i, ΔV_i), (p_i, $V_i - \Delta V_i$) and (p_i, $V_i + \Delta V_i$) are given in Figure 4. Essentially the PSDs overlap with each other suggesting uncertainty in the amount adsorbed actually has a minor influence on the intensity of the distributions and, as shown by the inset in Figure 4, negligible effect on the location of the maximum in each peak.

3.3.2. Effect of the regularization parameter on the PSD

For this analysis, the isotherm data were (p_i, V_i) only with optimized molecular model (Double LJ sites) and fixed number of SPIs. Regularization parameter, α, sensitivity was considered in two separate analyses: Firstly, PSD analysis of the (p_i, V_i) adsorption data set with selected α-values and secondly, α-values for the amounts adsorbed as (p_i, V_i) and (p_i, $V_i \pm \Delta V_i$). This latter analysis differs from that in Section 3.3.1 via use of optimized α-values for each data set compared with the application of the same α-value for all of the data sets in Section 3.3.1.

The error and GCV factor plots in Figure 2 shows their sensitivity to the α-value; the precise definition of the optimum value can be challenging. The shallow character of the GCV curve suggests it could be chosen from values varying between 1.0×10^{-7} and 1.0×10^{-6}. Fitting linear imprints onto the error curve and identifying their intersection, as suggested in Figure 2, may also approximate an optimum regularization parameter. Curvature in the imprinted linear sections would greatly impact on optimum regularization parameter selection.

The effect of α-value selection on PSD for a given set of adsorption data, (p_i,V_i), is shown in Figure 5. In this case, α was selected from the 4 pints bounded by 1.0×10^{-7} to 1.0×10^{-6}. Figure 5(a) shows the calculated PSD for each α and Figure 5(b) the resultant fitting to the experimental data. Figure 5(a) shows that there are relatively significant changes in the PSD with the apparently small changes in the α-value. Smaller α-values resulted in a spikier PSD.

The effects are seen here in two forms: the volume adsorbed in the width range 1.1-1.3 nm decreases with increasing α-value; for the smallest values in the set considered, pores are apparent at 1.5 nm but "disappear" for the α-value of 4.64×10^{-7}, the optimum value for the (p_i,V_i) data set. Interestingly, the overall fit to the isotherm data in Figure 5(b) is less sensitive to the α-value where the calculated isotherms fit reasonably closely to the (p_i, $V_i \pm \Delta V_i$), i.e. approximately within the uncertainty of the measured amounts adsorbed. This observation is somewhat expected on inspection of the generally shallow minimum in the GCV curve. A sharp minimum would give an opposite result.

We now contrast the uncertainty in amount adsorbed as a variable (Figure 4) with the effect in conjunction with regularization parameter, i.e. consider the effect of optimizing the α-value for the equivalent three isotherms as (p_i, V_i) and (p_i, $V_i \pm \Delta V_i$). The fitting was again made with the two-centre L-J model and the same number of SPIs for each isotherm data set. The result is shown in Figure 6. Distributions due to (p_i, V_i) and (p_i, $V_i + \Delta V_i$) are essentially equivalent with $\alpha=4.64\times10^{-7}$. In contrast, that due to (p_i, $V_i - \Delta V_i$), with $\alpha=2.15\times10^{-7}$, shows a slight increase in the peak intensity attributed to the smaller pore centered around 1.2 nm at the expense of those at 1.7 and 2.2 nm, with these larger pores showing an apparent narrowing in width.

Due to the lack of PSD sensitivity to the $u_C(V_i)$, we attribute these observations to the different α-values. The commercial equipment offering similar PSD analyses typically employ a list of default regularization parameters. Clearly, this observation implies a single α-value selection may be more of a guess and comparisons should be made with pre-conceived (or calculated) tolerance before any conclusions are drawn from the PSD results.

3.3.3. Effect of the molecular model of nitrogen on the PSD

To assess the effects of molecular probe-model on PSD, the (p_i, V_i) isotherm data set was fixed with the optimum α-value. The molecular model for nitrogen could be either a single (L-J) sphere model or a two-center L-J model. In the analyses to present, we only considered this latter model. For both molecular model analyses, we calculated and employed the same number (53) SPIs.

The nitrogen molecule consists of two nitrogen atoms connected through a triple bond and geometry more similar to a rod rather than a sphere. Considering the nitrogen molecule as single sphere (single L-J site) introduces at least two problems: 1. Since the parameters available for the spherical model are calculated statistically they are not as realistic as the double L-J center model; 2. The single sphere model presents a very different packing model to that for the rod-shaped, two-center model. The former results in a larger excluded volume and thus a more open structure than that due to the latter in pores of similar dimensions, across the micropore width range. Figure 7(a) shows calculated PSD based on both models. The PSD due to optimized conditions, i.e. the 2-center model contained 5 peaks in the range $0.80 \leq$ pore width ≤ 2.80 nm. The single-center model also gave 5 peaks with a primary peak centered at the same position as the former as 1.2 ± 0.1 nm. The position and intensity of the remaining 4 peaks are quite different, with the reduction in volume intensity for the primary peak accounted for by increases in the larger pores which are moved to slightly lower mean values, except for the largest pore at 2.3 nm which moved to approximately 2.5 nm. These changes are, on the whole, attributable to the difference in the model-dependent packing within the pores and the volume adsorbed matched via the SPIs.

The apparent modeling of the adsorption isotherm data for both models is shown in Figure 7(b). Again, the fit is very close to the uncertainty bounds of the measured data; an exception exists in the low-pressure range $1\times10^{-5}p^{o} \leq p \leq 5\times10^{-5}p^{o}$, due to the relatively low combined standard uncertainty in the amount adsorbed. The apparent fluctuations in the curve fit at the

higher pressures $5\times10^{-4}p^{o} \leq p \leq 1\times10^{-2}p^{o}$ are reflected in the differences in the PSD for pores > 1.30 nm.

3.3.4. Effect of the number of SPIs on the PSD

For this analysis, optimum regularization was used and the conditions maintained constant were: data set (p_i, V_i) and the two-center L-J model. A variation in the number of SPIs used in the overall isotherm data modeling has a considerable effect on the computing expense and application capacity.

The optimized number of SPIs for the (p_i, V_i) data fit was defined over the range 0.6-0.32 nm with a quadrature interval (Eq. (5)), w_j = 0.05 nm, giving 53 SPIs identified as Set 1. A second Set, 2, was defined with w_j = 0.1 nm giving 27 SPIs. Figure 8(a) shows the resulting PSDs. Set 2 SPIs suggests the adsorbent contains a bi-modal distribution as a primary peak mean width at 1.2 nm, but with decreased intensity and moderately wider range as 1.2 ± 0.2 nm, compared with 1.2 ± 0.1 nm for Set 1. A relatively broad, second peak is suggested at 2.3 ± 0.2 nm, with no indication of possible pores between these two ranges. Clearly, the smaller-valued quadrature interval provides scope for fitting (identifying) finer-grained pores within a material, interpreted as a higher-resolution PSD.

Figure 8(b) shows and compares the overall data fit across the isotherm. The loss of sensitivity due to the larger quadrature interval is again reflected in the relatively poorer fit compared with Set 1, with departures exceeding the combined standard uncertainty in the amount adsorbed. Overall, the smaller-valued interval gives a larger number of SPIs increasing the sensitivity and flexibility to fit the adsorption isotherm data.

Our analyses initially designed the optimum parameters for integral inversion of the adsorption data set (p_i, V_i). Such a procedure differs from (our understanding of) the commercial equipment methods where one method employs a macro to calculate the PSD using an optimized (but unspecified) α-value applied with (also unspecified) quadrature

interval and number of SPIs to fit the adsorption data. From a detailed inspection of the data fitting, the user could determine the approximate values for the quadrature interval and the number of applied SPIs. A second commercial approach is to provide an error curve from which the experimentalist selects the α-value by inspection but must also apply a fixed (unknown) quadrature interval and a suite of pre-calculated SPIs.

4. CONCLUSIONS

The sources of uncertainty likely to contribute to the combined standard uncertainty in the PSD are due to variations in the amount adsorbed, the value of the regularization parameter, the molecular model used to define the probe molecule, and the quadrature interval within a particular width range to generate a set of SPIs. Provided these parameters are optimized, a reasonable facsimile of the PSD could be expected.

Parametric analyses indicated where a decrease in PSD precision might occur:

a) On using optimized parameters for the (p_i, V_i) data set, the inclusion of the combined standard uncertainty in amount adsorbed had negligible effect on PSD reproducibility.

b) An inclusion of $u_C(V_i)$ affects regularization parameter optimization which, in turn, results in uncertainty in calculated PSD. A correct selection of the value of the regularization parameter was essential for identifying probable mean pore widths within a porous adsorbent containing relatively narrow and possibly specific pore widths. Reporting the value of regularization parameter used in the inversion calculations is encouraged;

c) The molecular model used to calculate the SPIs greatly influences the calculated PSD. The model used should be one that, as closely as possible, represents the physical shape as well as *intra* and *inter* atomic and/or molecular forces; and,

d) The quadrature interval value defines the number of SPIs to be used in the curve fitting of the adsorption data. The smaller the value, the larger the number of PSIs in a given pore range or width leading to a more detailed definition of pores within a given adsorbent. A smaller number of SPIs resulted in a decreased sensitivity to fit the adsorption isotherm data.

e) A quantitative comparison between calculated pore size distributions should be discouraged unless the uncertainty in the experimental data is relatively small and, the default value for the regularization parameter, the applied potential model, and the number of SPIs and their distribution are exactly the same for each pore size distribution evaluation.

ACKNOWLEDGMENTS

The authors thank the Australian Research Council discovery program (DP110101293) for funding support and S.H.M also thanks the University of South Australia for a postgraduate research scholarship**.**

REFERENCES

[1] F. Rouquerol, J. Rouquerol, K. Sing, Adsorption by powders and porous solids Academic Press, London, 1999.

[2] D.D. Do, H.D. Do, Pore characterization of carbonaceous materials by DFT and GCMC Simulations: A review, Adsorpt. Sci. Technol., 21 (2003) 389-423.

[3] D.D. Do, Adsorption Analysis: Equilibria and Kinetics, 1998.

[4] D. Frenkel, B. Smit, Understanding Molecular Simulation : From Algorithms to Applications., Academic Press., San Diego, 1996.

[5] J. Wu, Density functional theory for chemical engineering: From capillarity to soft materials, AIChE J., 52 (2006) 1169-1193.

[6] R. Evans, U.M.B. Marconi, P. Tarazona, Fluids in narrow pores: Adsorption, capillary condensation, and critical points, J. Phys. Chem., 84 (1986) 2376-2399.

[7] R. Evans, U.M.B. Marconi, P. Tarazona, Capillary condensation and adsorption in cylindrical and slit-like pores, J. Chem. Soc., Farad. T. 2, 82 (1986) 1763-1787.

[8] N.A. Seaton, J.P.R.B. Walton, N. quirke, A new analysis method for the determination of the pore size distribution of porous carbons from nitrogen adsorption measurements, Carbon, 27 (1989) 853-861.

[9] C. Lastoskie, K.E. Gubbins, N. Quirke, Pore size distribution analysis of microporous carbons: a density functional theory approach, J. Phys. Chem., 97 (1993) 4786-4796.

[10] P. Tarazona, Free-energy density functional for hard spheres, Phys. Rev. A, 31 (1985) 2672-2679.

[11] ISO-15901-3, Pore size distribution and porosity of solid materials by mercury porosimetry and gas adsorption in analysis of micropores by gas adsorption, 2007.

[12] P.I. Ravikovitch, A.V. Neimark, Density functional theory model of adsorption on amorphous and microporous silica materials, Langmuir, 22 (2006) 11171-11179.

[13] A.V. Neimark, Y. Lin, P.I. Ravikovitch, M. Thommes, Quenched solid density functional theory and pore size analysis of micro-mesoporous carbons, Carbon, 47 (2009) 1617-1628.

[14] G.Y. Gor, M. Thommes, K.A. Cychosz, A.V. Neimark, Quenched solid density functional theory method for characterization of mesoporous carbons by nitrogen adsorption, Carbon, 50 (2012) 1583-1590.

[15] J. Landers, G.Y. Gor, A.V. Neimark, Density functional theory methods for characterization of porous materials, Colloid. Surface A., 437 (2013) 3-32.

[16] W.V. Loebenstein, V.R. Deitz, The magnitude of the experimental error in the adsorption of nitrogen at 78 K on various surfaces, The J. Chem. Phys., 15 (1947) 687-688.

[17] S. Ross, J.P. Olivier, On physical adsorption, Interscience Publishers, Sydney, 1964.

[18] E. Robens, J.U. Keller, C.H. Massen, R. Staudt, Sources of error in sorption and density measurements, J. Therm. Anal. Calorim., 55 (1999) 383-387.

[19] G.R. Killip, R.W. Camp, J. Orr, C., Temperature controlling apparatus for use with pore volume and surface area analyzers Re-issued U.S. Patent 33,567, April 9, 1991 (original U.S. Patent 4,693,124, September 15 1987).

[20] A. Badalyan, P. Pendleton, H. Wu, Development of an automated gas adsorption apparatus for the characterization of the surface area, pore size distribution, and density of powdered materials, Rev. Sci. Instrum., 72 (2001) 3038-3045.

[21] A. Badalyan, P. Pendleton, Analysis of uncertainties in manometric gas-adsorption measurements. I: Propagation of uncertainties in BET analyses, Langmuir, 19 (2003) 7919-7928.

[22] A. Badalyan, P. Pendleton, Uncertainty in α_s analyses and pore volumes propagated from uncertainty in gas adsorption data, in: P.L. Llewellyn, F. Rodriquez-Reinoso, J. Rouqerol, N. Seaton Stud. Surf. Sci. Catal., Elsevier, 2007, pp. 383-388.

[23] A. Badalyan, P. Pendleton, Analysis of uncertainties in manometric gas-adsorption measurements: II. Uncertainty in -analyses and pore volumes, J. Colloid Interface Sci., 326 (2008) 1-7.

[24] J.N. Caguiat, D.W. Kirk, C.Q. Jia, Uncertainties in characterization of nanoporous carbons using density functional theory-based gas physisorption, Carbon, 72 (2014) 47-56.

[25] S.H. Madani, A. Badalyan, M.J. Biggs, P. Pendleton, Uncertainty in pore size distribution derived from adsorption isotherms: I. Classical methods, submitted for Micropor. Mesopor. Mat., (2014).

[26] A. Badalyan, R. Bromball, P. Pendleton, W. Skinner, An assessment of activated carbon cloth microporosity change due to chemical activation, Carbon, 48 (2010) 1004-1011.

[27] A. Wongkoblap, D.D. Do, Characterization of Carbot Non-Graphitized Carbon Blacks with a Defective Surface Model: Adsorption of Argon and Nitrogen, Carbon, 45 (2007) 1527-1534.

[28] L.F. Herrera, D.D. Do, G.R. Birkett, Histogram of number of particles as an indicator for 2D phase transition in adsorption of gases on graphite, Mol. Simulat., 36 (2010) 1173-1181.

[29] G.M. Davies, N.A. Seaton, V.S. Vassiliadis, Calculation of pore size distributions of activated carbons from adsorption isotherms, Langmuir, 15 (1999) 8235-8245.

[30] P.H. Merz, Determination of adsorption energy distribution by regularization and a characterization of certain adsorption isotherms, J. Comput. Phys., 38 (1980) 64-85.

[31] M.V. Szombathely, P. Bräuer, M. Jaroniec, The solution of adsorption integral equations by means of the regularization method, J. Comput. Chem., 13 (1992) 17-32.

[32] J.D. Wilson, Statistical approach to the solution of first-kind integral equations arising in the study of materials and their properties, J. Mater. Sci., 27 (1992) 3911-3924.

[33] K.S.W. Sing, D.H. Everett, R.A.W. Haul, L. Moscou, R.A. Pierotti, J. Rouquerol, T. Siemieniewska, Reporting physisorption data for gas/solid systems with special reference to the determination of surface area and porosity, Pure Appl. Chem., 57 (1985) 603.

[34] J. Jagiello, Stable numerical solution of the adsorption integral equation using splines, Langmuir, 10 (1994) 2778-2785.

FIGURE CAPTIONS

Figure 1. Adsorption isotherm of nitrogen on the microporous ACC FM1/250 at 77K; the inset amplifies the data points showing the combined standard uncertainty in the amount adsorbed as V_i and $V_i \pm \Delta V_i$

Figure 2. Guides for optimum regularization parameter selection; GCV score function (—) and fitting error (– –)

Figure 3. PSD derived from the nitrogen isotherm at 77K. The figure was calculated via an optimum-valued regularization parameter $\alpha = 4.64\times10^{-7}$ and the double size and charges model to simulate the nitrogen SPIs

Figure 4. Effect of the uncertainty on the adsorption amount on PSD; $V–\Delta V$ (– –), V (—),$V+\Delta V$ (•••)

Figure 5. Effect of the regularization parameter on PSD (a) and isotherm fitting (b); $\alpha=1\times10^{-7}$ (—), $\alpha=2.15\times10^{-7}$ (– –), $\alpha=4.64\times10^{-7}$ (•••), $\alpha=1\times10^{-6}$ (–•–), experimental data (▬)

Figure 6. PSD calculated from $V-\Delta V$ (– –), V (—),$V+\Delta V$ (•••) and using the optimum regularization parameter at each case

Figure 7. Effect of the potential model on the calculated PSD (a) and isotherm fitting (b); data derived from double LJ potential (—), single LJ (– –) potential, and experimental data (▬)

Figure 8. Effect of the number of SPIs on PSD (a) and isotherm fitting (b); set 1 with 0.05 nm interval between SPIs (—), set 2 with 0.1 nm interval between SPIs (– –), experimental data (▬)

FIGURES

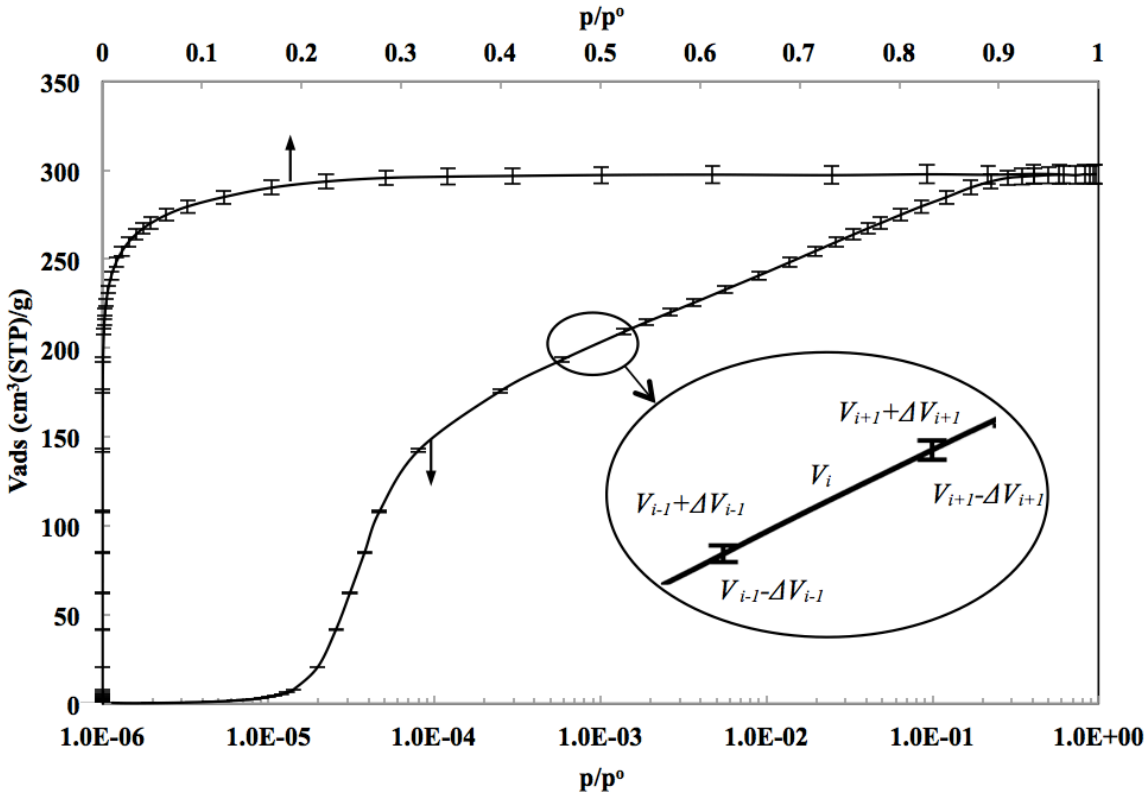

Figure 1. Adsorption isotherm of nitrogen on the microporous ACC FM1/250 at 77K; the inset amplifies the data points showing the combined standard uncertainty in the amount adsorbed as V_i and $V_i \pm \Delta V_i$

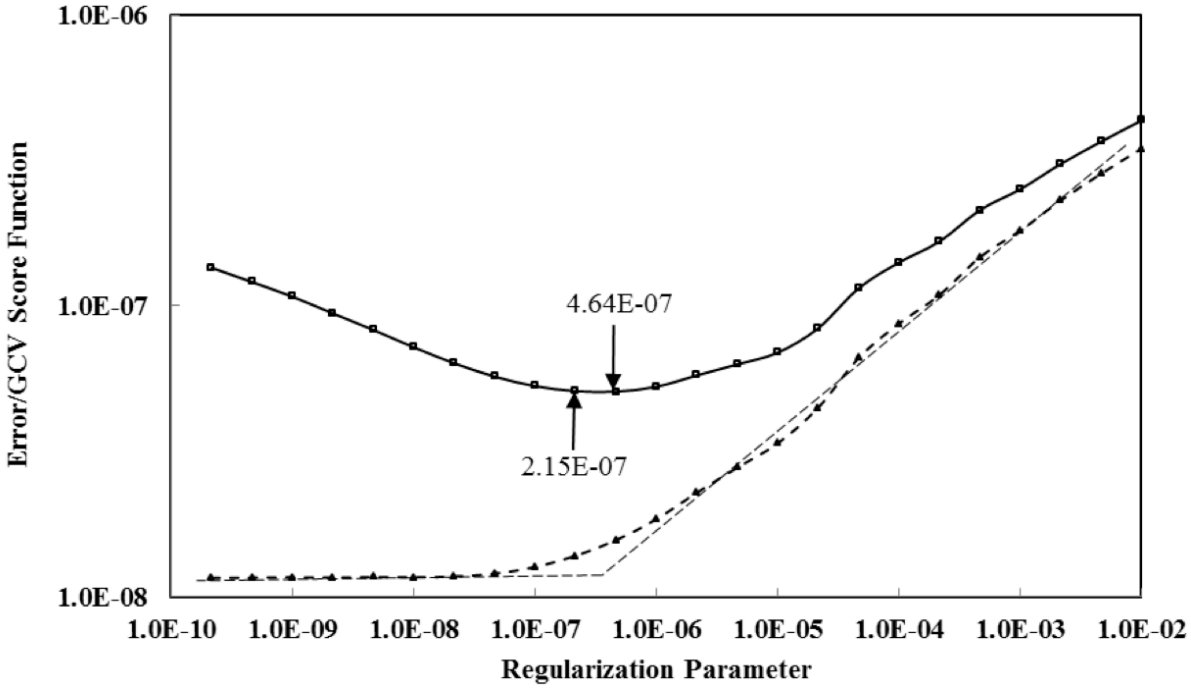

Figure 2. Guides for optimum regularization parameter selection; GCV score function (─) and fitting error (– –)

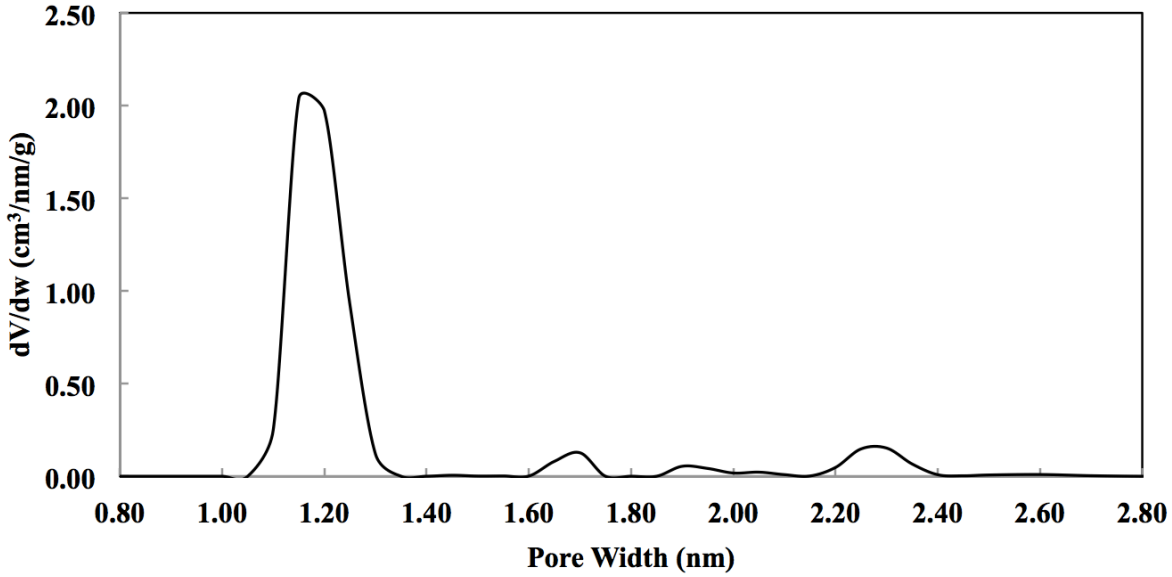

Figure 3. PSD derived from the nitrogen isotherm at 77K. The figure was calculated via an optimum-valued regularization parameter $\alpha = 4.64\times10^{-7}$ and the double size and charges model to simulate the nitrogen SPIs

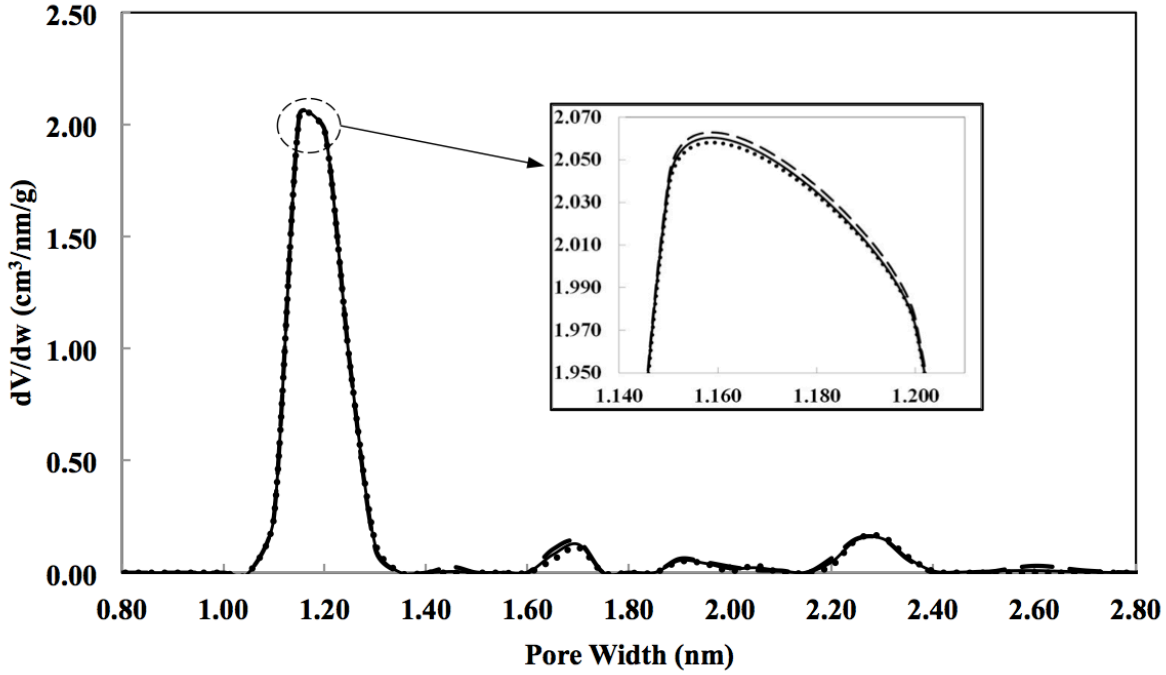

Figure 4. Effect of the uncertainty on the adsorption amount on PSD; $V-\Delta V$ (– –), V (—), $V+\Delta V$ (•••)

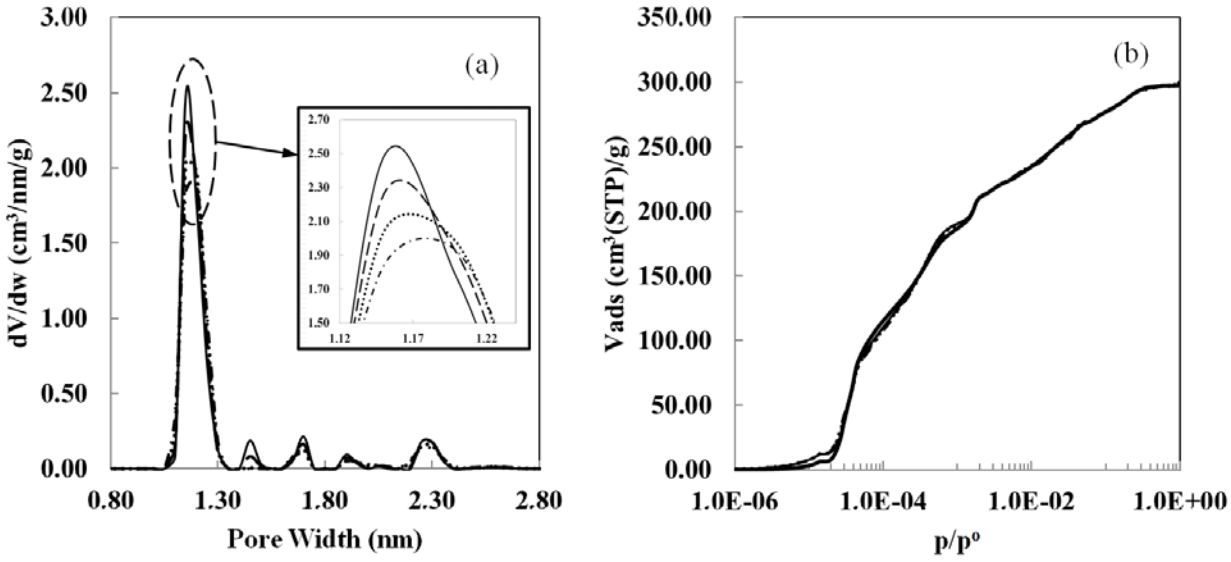

Figure 5. Effect of the regularization parameter on PSD (a) and isotherm fitting (b); $\alpha=1\times10^{-7}$ (—), $\alpha=2.15\times10^{-7}$ (– –), $\alpha=4.64\times10^{-7}$ (•••), $\alpha=1\times10^{-6}$ (–•–), experimental data (▬)

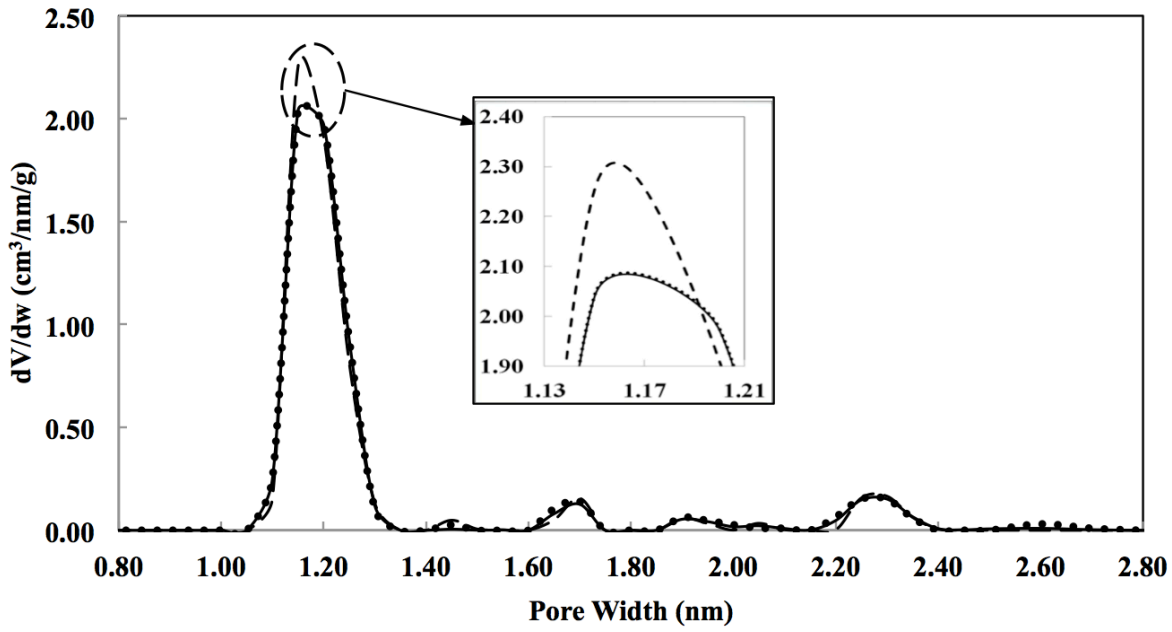

Figure 6. PSD calculated from V-ΔV (– –), V (—),V+ΔV (•••) and using the optimum regularization parameter at each case

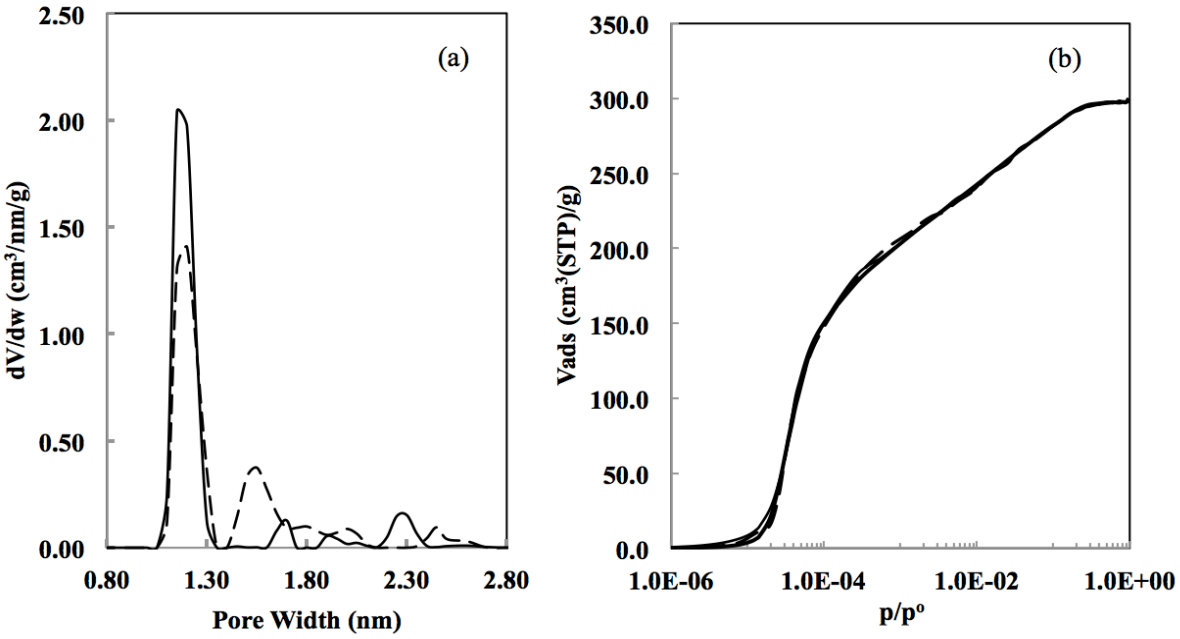

Figure 7. Effect of the potential model on the calculated PSD (a) and isotherm fitting (b); data derived from double LJ potential (—), single LJ (– –) potential, and experimental data (—)

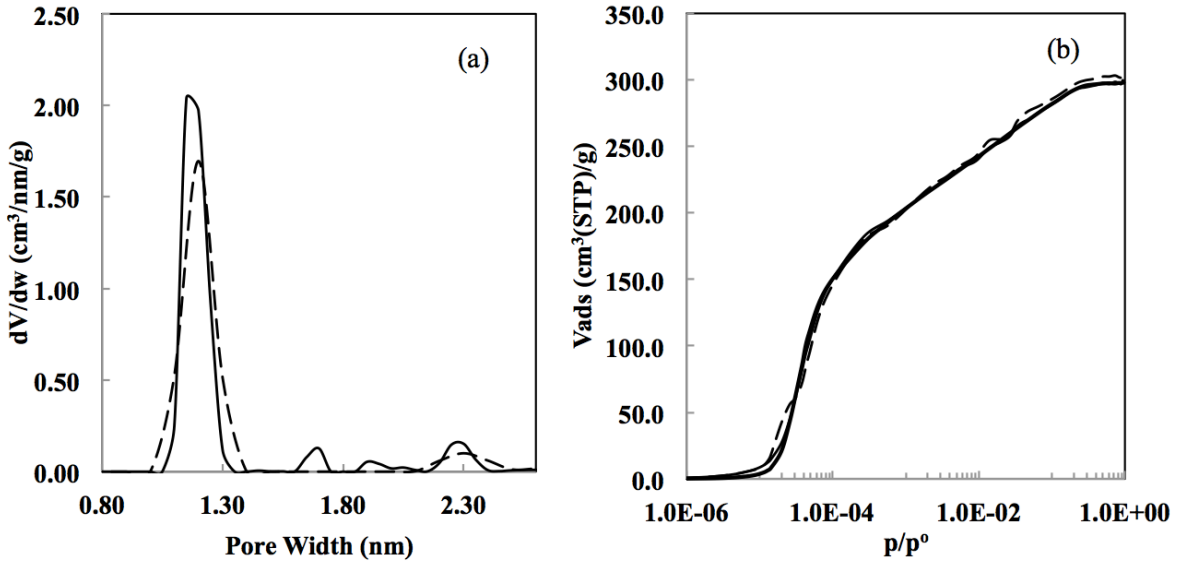

Figure 8. Effect of the number of SPIs on PSD (a) and isotherm fitting (b); set 1 with 0.05 nm interval between SPIs (─), set 2 with 0.1 nm interval between SPIs (– –), experimental data (**▬**)